Traumatic Joint Injury Induces Acute Catabolic Bone Turnover Concurrent with Articular Cartilage Damage in a Rat Model of Post-Traumatic Osteoarthritis

— Source link ↗

Tristan Maerz, Michael D. Newton, Mackenzie M Fleischer, Samantha E. Hartner ...+4 more authors

Institutions: University of Michigan, Beaumont Health, Oakland University

Related papers:

- Traumatic joint injury induces acute catabolic bone turnover concurrent with articular cartilage damage in a rat model of posttraumatic osteoarthritis

- Subchondral and trabecular bone remodeling in canine experimental osteoarthritis.

- Characterization of articular cartilage and subchondral bone changes in the rat anterior cruciate ligament transection and meniscectomized models of osteoarthritis.

- Subchondral bone sclerosis and cancellous bone loss following OA induction depend on the underlying bone phenotype

- Alterations in subchondral bone plate, trabecular bone and articular cartilage properties of rabbit femoral condyles at 4 weeks after anterior cruciate ligament transection.

1   **Traumatic Joint Injury Induces Acute Catabolic Bone Turnover Concurrent with**

2   **Articular Cartilage Damage in a Rat Model of Post-Traumatic Osteoarthritis**

3

4   Tristan Maerz[1], Michael D. Newton[2], Mackenzie Fleischer[2], Samantha E. Hartner[2],

5   Karissa Gawronski[1], Lucas Junginger[1], *Kevin C. Baker[2,3]

6

7   [1]Department of Orthopaedic Surgery, University of Michigan, Ann Arbor, MI

8   [2]Orthopaedic Research Laboratory, Beaumont Health, Royal Oak, MI

9   [3]Department of Orthopaedic Surgery, Oakland University William Beaumont School of

10   Medicine, Rochester, MI

11

12   **Running Title:** Catabolic Bone Turnover after ACL Rupture

13   **Disclosure:** None of the authors have any relevant financial conflict with the content of this

14   work.

15

16   ***Corresponding Author:**

17   Kevin C. Baker, PhD

18   3811 W Thirteen Mile Road

19   Royal Oak, MI 48073

20   Phone Number: 248-551-9177

21   Fax Number: 248-551-0191

22   E-Mail: kevin.baker@beaumont.edu

23

24   **ABSTRACT**

25   **Objective:** Assess acute alterations in bone turnover, microstructure, and histomorphometry following

26   noninvasive anterior cruciate ligament rupture (ACLR).

27   **Methods:** Twelve female Lewis rats were randomized to receive noninvasive ACLR or Sham loading

28   (n=6/group). I*n vivo* μCT was performed at 3, 7, 10, and 14 days post-injury to quantify compartment-

29   dependent subchondral (SCB) and epiphyseal trabecular bone remodeling. Near-infrared (NIR) molecular

30   imaging was used to measure *in vivo* bone anabolism (800 CW BoneTag) and catabolism (Cat K 680

31   FAST). Metaphyseal bone remodeling and articular cartilage morphology was quantified using *ex vivo*

32   μCT and contrast-enhanced μCT, respectively. Calcein-based dynamic histomorphometry was used to

33   quantify bone formation. OARSI scoring was used to assess joint degeneration, and osteoclast number

34   was quantified on TRAP stained-sections.

35   **Results:** ACLR induced acute catabolic bone remodeling in subchondral, epiphyseal, and metaphyseal

36   compartments. Thinning of medial femoral condyle (MFC) SCB was observed as early as 7 days post-

37   injury, while lateral femoral condyles (LFC) exhibited SCB gains. Trabecular thinning was observed in

38   MFC epiphyseal bone, with minimal changes to LFC. NIR imaging demonstrated immediate and

39   sustained reduction of bone anabolism (~15-20%), and a ~32% increase in bone catabolism at 14 days,

40   compared to contralateral limbs. These findings were corroborated by reduced bone formation rate and

41   increased osteoclast numbers, observed histologically. ACLR-injured femora had significantly elevated

42   OARSI score, cartilage thickness, and cartilage surface deviation.

43   **Conclusion:** ACL rupture induces immediate and sustained reduction of bone anabolism and

44   overactivation of bone catabolism, with mild-to-moderate articular cartilage damage at 14 days post-

45   injury.

46

47

48   **INTRODUCTION:**

49   Post-traumatic osteoarthritis (PTOA) is a degenerative joint condition known to develop

50   following traumatic joint injuries. Anterior cruciate ligament (ACL) rupture is associated with a

51   particularly high risk for PTOA development – approximately 50% of patients develop PTOA

52   10-15 years after ACL rupture[1-3]. Surgical ACL reconstruction is a successful treatment to

53   alleviate pain and restore joint stability and function, but despite excellent patient-reported

54   outcomes and a high return-to-sport incidence, reconstruction has not been definitively shown to

55   alter the natural history of PTOA[2, 4, 5]. This observation has led to the hypothesis that acute

56   biological events initiated post-injury play a key role in the onset and progression of PTOA, as

57   opposed to primarily chronic joint instability. These biological events, their respective

58   contribution to PTOA pathogenesis, and the mechanisms that regulate them remain poorly

59   understood.

60   Crosstalk between articular cartilage (AC) and bone is an important component of

61   healthy joint homeostasis. AC and underlying bone interact via biochemical and mechanical

62   mechanisms, and subchondral bone (SCB) is responsible for mediating the nutritional supply of

63   AC[6]. In both OA and PTOA, the osteochondral unit undergoes dynamic degenerative changes[7, 8]

64   and increased biochemical crosstalk is hypothesized to drive SCB remodeling, vascular invasion

65   of deep cartilage, and chondrocyte hypertrophy[9-12]. Recent clinical and preclinical studies

66   suggest that alterations in SCB structure and composition may precede detectable damage in AC

67   in idiopathic OA[13-16], however this has not been shown for PTOA specifically. In PTOA, bony

68   alterations manifest dynamically and are characterized by both lytic and sclerotic phenotypes;

69   SCB loss is observed in the acute timeframe after injury and has been associated with

70   inflammation-mediated osteoclastogenesis and limb offloading due to injury-related gait

71   changes[17, 18]. Chronically, SCB undergoes sclerosis, a classical symptom of radiographic OA

72   recently associated with overactivation of Wnt/β-catenin signaling[19-21].

73   Studies of preclinical PTOA have demonstrated rapid loss of SCB and epiphyseal

74   trabecular bone following ACL injury[18, 22-24]. In a murine model of noninvasive ACL rupture-

75   induced PTOA, epiphyseal trabecular bone loss was observed as early as 1-week post-injury,

76   characterized by decreased bone volume fraction, bone mineral density, and trabecular

77   thickness[18, 22]. Using a rat model of noninvasive ACL rupture, our group has demonstrated a

78   similar phenotype of subchondral and epiphyseal trabecular bone loss at intermediate (4-week)

79   and chronic (10-week) timepoints[25]. However, no study has longitudinally characterized bone

80   remodeling *in vivo* acutely after injury, and it remains unclear whether it is associated with

81   dampened bone formation, increased bone resorption, or both. To this end, the purpose of this

82   study was to use *in vivo* imaging, structural histology, and dynamic histomorphometry to

83   characterize acute changes to bone deposition, bone resorption, and bone microstructure in a

84   noninvasive rat model of ACL rupture. Further, we sought to employ quantitative contrast-

85   enhanced μCT and histological evaluation of AC to contextualize bone-related findings with AC

86   degeneration and demonstrate whether acute alterations in bone precede measurable AC changes.

87   We hypothesized that bone anabolism is thwarted and bone resorption (i.e. osteoclast activity) is

88   increased immediately following joint injury, and that major structural changes in SCB and

89   epiphyseal trabecular bone precede marked AC degeneration.

90   **METHODS:**

91   *Animals and Induction of Noninvasive ACL Rupture*

92   Following institutional animal care and use committee approval, twelve female Lewis

93   rats aged 14 weeks, ~200-220g (Charles River Laboratories, Wilmington, MA, USA) were

94   randomized to ACL rupture (ACLR) or sham injury (Sham) (n=6/group). Sample size was

95   determined based on μCT data from our prior studies using this rat model[25] based on detection of

96   a 5% difference in trabecular bone volume fraction between groups (effect size=2.2, α=0.05,

97   power=0.9). Immediately prior to injury, rats were administered 5 mg/kg subcutaneous

98   Carprofen, anesthetized with intraperitoneal ketamine/xylazine, and maintained under 1-2%

99   inhaled isoflurane. Noninvasive ACLR was induced using tibial compression-based mechanical

100   loading, as previously described[25-27]. Rats were positioned prone on a custom fixture, with the

101   right knee in ~100° of flexion. Following preloading (3 N) and preconditioning (1-5 N), a rapid

102   3.0 mm displacement was applied to the tibia using a mechanical testing system (Insight 5, MTS

103   Systems, Eden Prairie, MN, USA), resulting in a closed, isolated ACL rupture. Sham rats

104   underwent preload and preconditioning only, without 3-mm injury loading. Following loading,

105   animals were administered the anesthetic reversal agent yohimbine (0.2 mg/kg SC). Rats were

106   allowed *ad libidum* cage activity in a 12-hr light/dark facility. To enable dynamic

107   histomorphometric assessment of bone formation, rats received intraperitoneal injections of 1%

108   calcein solution buffered with $NaHCO_3$ at the time of injury and 24 hrs prior to CO_2 asphyxia-

109   induced euthanasia 14 days post-injury.

110   *Near Infrared (NIR) Molecular Imaging to Assess Bone Deposition and Resorption*

111   At 3, 7, 10, and 14 days post-injury, rats underwent *in vivo* near-infrared fluorescence

112   (NIR) molecular imaging to longitudinally quantify bone deposition. Twenty-four hours prior to

113   imaging, rats received 5 nmol intravenous IRDye 800 CW BoneTag (BoneTag) (LI-COR,

114   Lincoln, NE, USA). BoneTag is a calcium-chelating fluorescent compound that incorporates into

115   newly mineralized bone, enabling *in vivo* assessment of bone formation[28]. At the 14-day

116   timepoint, to assess *in vivo* osteoclast activity as a measure of bone resorption, rats received 5

117   nmol Cat K 680 FAST (CatK) (PerkinElmer, Waltham, MA, USA). CatK is an activatable

118   fluorescent probe that detects *in vivo* Cathepsin K activity, an indirect measure of osteoclast

119   activity[29, 30]. On the day of imaging, lower limb fur was removed, and lateral NIR images of both

120   hindlimbs were acquired in the 700 and 800 nm channels (Pearl Impulse, LI-COR) under

121   isoflurane-induced anesthesia. Consistently-sized regions of interest (ROIs) were virtually placed

122   onto each knee (Fig 3A), and mean fluorescent intensity was calculated within each ROI. To

123   control for compounding BoneTag signal and animal-to-animal variability, normalized BoneTag

124   and CatK signals were calculated by dividing mean fluorescent intensity of the ACLR

125   injured/Sham uninjured limb by its respective contralateral limb.

126   *μCT Imaging*

127   Rats underwent live, bilateral *in vivo* μCT imaging of the distal femoral epiphysis at 3, 7,

128   10, and 14 days post-injury (55 kVp, 114 μA,15.6 μm voxel, Viva-80, Scanco Medical AG,

129   Brüttisellen, Switzerland) under isoflurane-induced anesthesia. Following euthanasia at 14 days,

130   distal femora were harvested and meticulously dissected under microscopy to expose AC,

131   facilitating subsequent contrast-enhanced μCT of AC. Femora were fixed in 10% neutral

132   buffered formalin for 72 hrs and stored in 70% ethanol. At the time of *ex vivo* imaging, femora

133   were rehydrated in PBS for 24 hrs. Distal femoral metaphyses were imaged using *ex vivo* μCT

134   (55 kVp, 145μA, 6 μm voxel, μCT-40, Scanco Medical), as longitudinal *in vivo* imaging was not

135   possible due to live imaging time limitations. Femora were then incubated in 20% ioxaglate

136   (Hexabrix 320, Guerbet LLC, Princeton, NJ), pH=7.2 for 24 hrs, and contrast-enhanced μCT

137   imaging of AC was acquired (55 kVp, 145μA, 8 μm voxel). All *ex vivo* imaging was performed

138   in a humidified sample holder.

139   *μCT Image Analysis*

140   Image processing and analysis was performed using MATLAB (Mathworks Inc., Natick,

141   MA, USA). All manual tissue contouring was performed by the lead author (TM). Standardized

142   bone morphometry parameters were calculated using the ImageJ plug-in BoneJ[31], utilizing the

143   MATLAB–ImageJ interface Miji[32].

144   To enable accurate voxel-by-voxel characterization of longitudinal bone remodeling, a

145   semi-automated registration algorithm was used to segment epiphyseal trabecular bone and SCB

146   from *in vivo* μCT images. First, epiphyseal trabecular bone and AC were segmented from

147   endpoint contrast-enhanced μCT via manual contouring and automated, registration-based

148   segmentation (described below), respectively. Contrast-enhanced μCT scans for each limb were

149   rigidly registered onto respective *in vivo* μCT data sets, enabling mapping of epiphyseal bone

150   and AC volumes across longitudinal data. SCB was segmented by dilating AC volumes and

151   thresholding bone, as previously described[25]. Metaphyseal trabecular bone was manually

152   contoured from *ex vivo* μCT images. BV/TV, BMD, TMD, Tb.Th, Tb.N, and Tb.Sp were

153   calculated for epiphyseal and metaphyseal trabecular bone volumes, while BV/TV, BMD, TMD,

154   and SCB.Th were calculated for SCB volumes.

155   AC volumes were segmented from contrast-enhanced μCT images using a custom, atlas-

156   based registration scheme (data not published; manuscript under revision; expected publication

157   June 2020). Briefly, an average tissue atlas of the distal femur was generated from a population

158   of manually segmented training images. The averaging process yields an atlas with pre-defined

159   tissue boundaries and averaged anatomy, enabling robust and highly accurate registration onto

160   both healthy and injured femora (Dice Similarity Coefficient > 0.95). This atlas was registered

161   onto contrast-enhanced µCT images, followed by thresholding to remove residual air and bone,

162   to segment AC. Registrations were inspected by an expert (MDN) to confirm accurate

163   segmentation. AC morphology was analyzed by mean cartilage thickness (MCT) and surface

164   deviation (S_a), as previously shown by our group[26, 33]. In brief, the bone-cartilage interface was

165   isolated from final AC volumes and mapped from 3D to 2D using conformal parameterization[34],

166   enabling the generation of 2D AC thickness maps, from which MCT and S_a can be derived.

167   *Structural Histology and Dynamic Histomorphometry*

168   Fixed femora were processed for undecalcified histology and embedded in polymethyl

169   methacrylate. Spaced 6-µm sagittal sections of the medial femoral condyle (MFC) and lateral

170   femoral condyle (LFC) were cut and stained with Safranin-O/Fast Green (Saf-O). Adjacent

171   unstained sections at each interval were cut and mounted for fluorescent imaging of calcein to

172   quantify bone formation. Further sections at each interval were stained for tartrate-resistant acid

173   phosphatase (TRAP) to identify osteoclasts. Brightfield imaging was performed at 20x using an

174   automatic slide imaging system (Aperio, Leica 122 Biosystems, Buffalo Grove, IL, USA).

175   Fluorescent imaging of calcein labeling was performed using standard FITC fluorescent

176   microscopy at 10x magnification (Eclipse E800, Nikon, Tokyo, Japan).

177   To assess osteoarthritis severity, Saf-O stained sections were evaluated by two blinded

178   investigators using the Osteoarthritis Research Society International (OARSI) score[35]. OARSI

179   scores of the MFC and LFC were evaluated both separately and together as an average score.

180   Static and dynamic histomorphometric parameters were quantified in a blinded fashion using the

181   Bioquant Osteo software (Bioquant Image Analysis Corp., Nashville, TN), according to standard

182   procedures[36]. In brief, Saf-O sections were used to quantify static measures (BV, TV, and BS) in

183   epiphyseal trabecular bone. Adjacent unstained fluorescent sections were used to measure

184   calcein labels to derive dynamic measures of bone formation within the 14-day study period,

185   namely total mineralizing surface (MS), mineralizing surface over bone surface (MS/BS),

186   mineral apposition rate (MAR), bone formation rate over bone volume (BFR/BV). An important

187   distinction in these parameters is that MAR and BFR/BV are measures of bone formation

188   kinetics (directly related to the inter-label distance of calcein bands), whereas MS/BS assesses

189   the proportion of actively mineralizing bone independent of bone formation rates (independent of

190   inter-label distance). Lastly, TRAP$^+$ osteoclasts were segmented from TRAP-stained sections

191   using image analysis, and osteoclast number per total area (N.Oc/T.Ar) and osteoclast number

192   per bone surface (N.Oc/BS) were quantified.
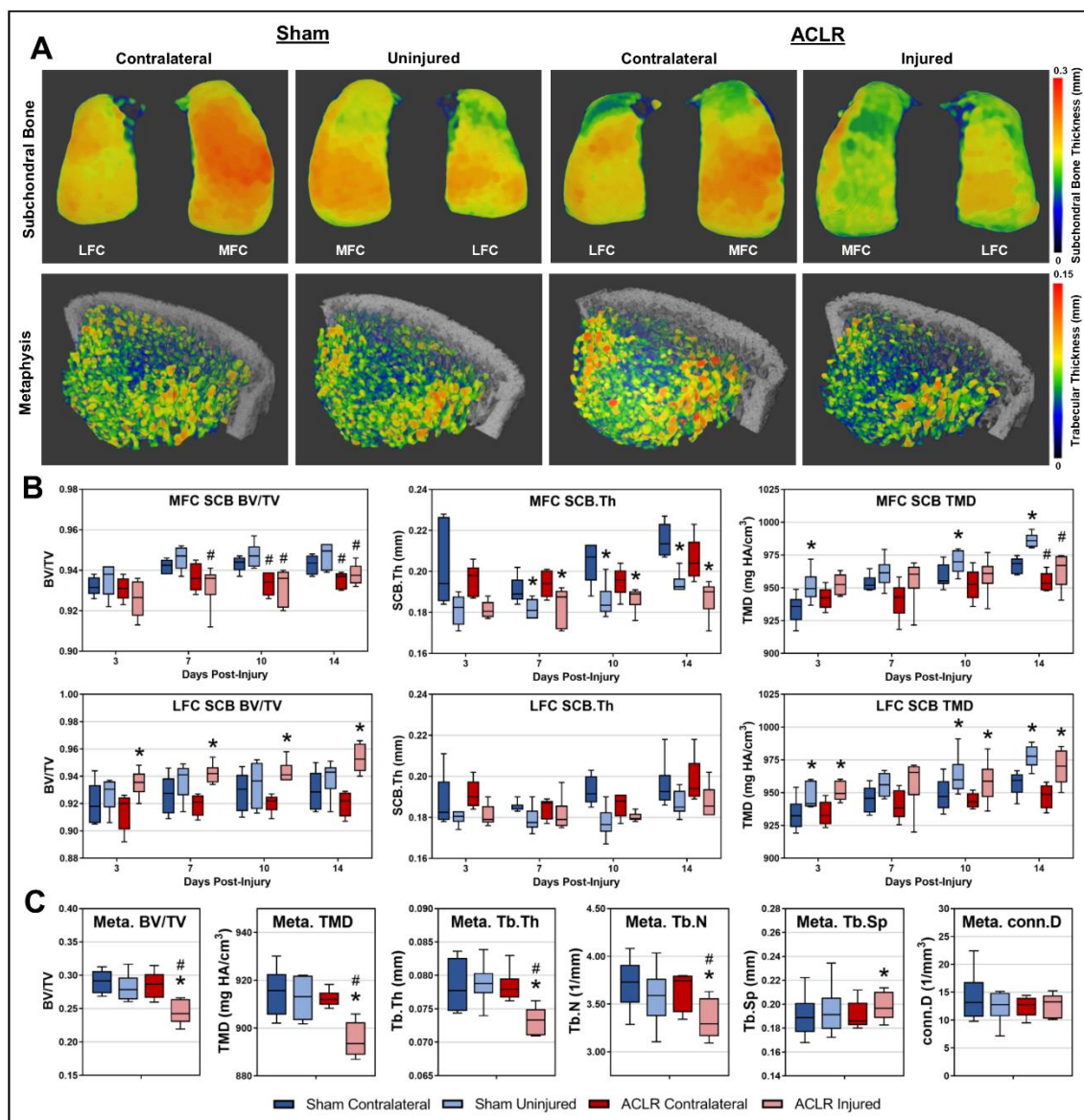
193   *Data Analysis and Statistics*

194   Statistical analyses were performed in SPSS (v22, IBM, Armonk, NY). Normality and

195   equal variance assumptions were confirmed and appropriately addressed in all continuous data.

196   Longitudinal *in vivo* data was analyzed between Sham and ACLR groups and between

197   injured/uninjured and contralateral limbs using a linear mixed model, with "group" as a between-

198   subject factor and "limb/laterality" and "time" as within-subject factors. This analysis enabled us

199   to sensitively elucidate longitudinal trends by appropriately accounting for within-subject and

200   between-subject variance. *Ex vivo*/endpoint μCT data was analyzed by two-way analysis of

201   variance (ANOVA), with "group" as a between-subject factor and "limb/laterality" as a within-

202   subject factor. Multiple comparisons were performed with Sidák P-value correction. Ordinal data

203   was compared using Kruskal-Wallis tests with a Dunn's *post-hoc* comparison correction.

204   Bivariate correlations were performed using Pearson correlations. Adjusted P-values less than

205   0.05 were considered significant.

206   **RESULTS:**

207   *ACL Rupture Induced Progressive and Compartment-Dependent Subchondral Bone Alterations*

208   Aging-related gradual increases in SCB BV/TV, TMD, and SCB.Th are evident in the

209   Sham group (Fig 1B). ACLR induced longitudinal loss of SCB BV/TV and SCB.Th (Fig 1B),

210   and, unexpectedly, sham-loaded rats also exhibited significantly lower SCB.Th compared to their

211   respective contralateral femora, albeit to a lesser degree than ACLR (Fig 1B). SCB thinning of

212   the MFC in Sham uninjured limbs was confined to the anterior condyle, whereas the MFC in

213   injured ACLR limbs exhibited thinning through the entire condyle (Fig 1A). By the 14d

214   timepoint, injured knees in ACLR had significantly lower SCB BV/TV and TMD compared to

215   uninjured knees in Sham. On the LFC, injured ACLR femora exhibited progressive SCB BV/TV

216   gains compared to contralateral knees, and loaded knees in both Sham and ACLR exhibited SCB

217   TMD gains (Fig 1B).

218

Fig 1. Subchondral and Metaphyseal Bone Morphometry. Three-dimensional thickness maps

demonstrate compartment-dependent alterations in SCB morphometry and catabolic remodeling

of metaphyseal trabecular bone following ACLR (A). Compared to Sham, ACLR had lower SCB

BV/TV and TMD on the MFC in both limbs, whereas the LFC of injured ACLR knees exhibited

BV/TV and TMD gains (n=6 Sham; n=5 ACLR) (B). Both ACLR and Sham induced SCB

thinning on the MFC, compared to contralateral knees (B). MFC thinning in Sham was confined

to the anterior condyle, whereas the ACLR MFC exhibits thinning throughout the entire condyle

(B). ACLR also induced catabolic remodeling of metaphyseal trabecular bone (n=6 Sham; n=6

227   ACLR) (A,C). * indicates significant difference to contralateral limb; # indicates significant

228   difference to ipsilateral limb in Sham.

229

230   *ACL Rupture Induced Catabolic Remodeling of Femoral Metaphyseal and Epiphyseal*

231   *Trabecular Bone*

232   Compared to both contralateral ACLR femora and uninjured Sham femora, injured

233   ACLR femora exhibited significantly lower metaphyseal BV/TV, TMD, BMD, and Tb.Th. (Fig

234   1) at the 14d endpoint. Injured ACLR femora also had significantly lower metaphyseal Tb.N and

235   significantly higher Tb.Sp compared to uninjured contralateral femora.

236   Longitudinal μCT imaging of epiphyseal bone revealed a progressively catabolic

237   phenotype in the MFC and LFC following ACLR, with the most pronounced changes in the

238   MFC (Fig 2). Significant decreases in trabecular BV/TV and Tb.Th of the injured ACLR MFC

239   were observed by the 10d and 14d timepoints (Fig 2), and loss of BV/TV was also observed on

240   the LFC as early as 10d. Both femora in ACLR exhibited decreased epiphyseal TMD compared

241   to respective limbs in Sham, likely due to reduced activity in ACLR rats. Injured ACLR femora

242   exhibited significantly, albeit marginally increased Tb.N in the MFC. No changes in Tb.Th,

243   Tb.N, or Tb.Sp were noted in the LFC in any femora in ACLR or Sham (Fig 2).
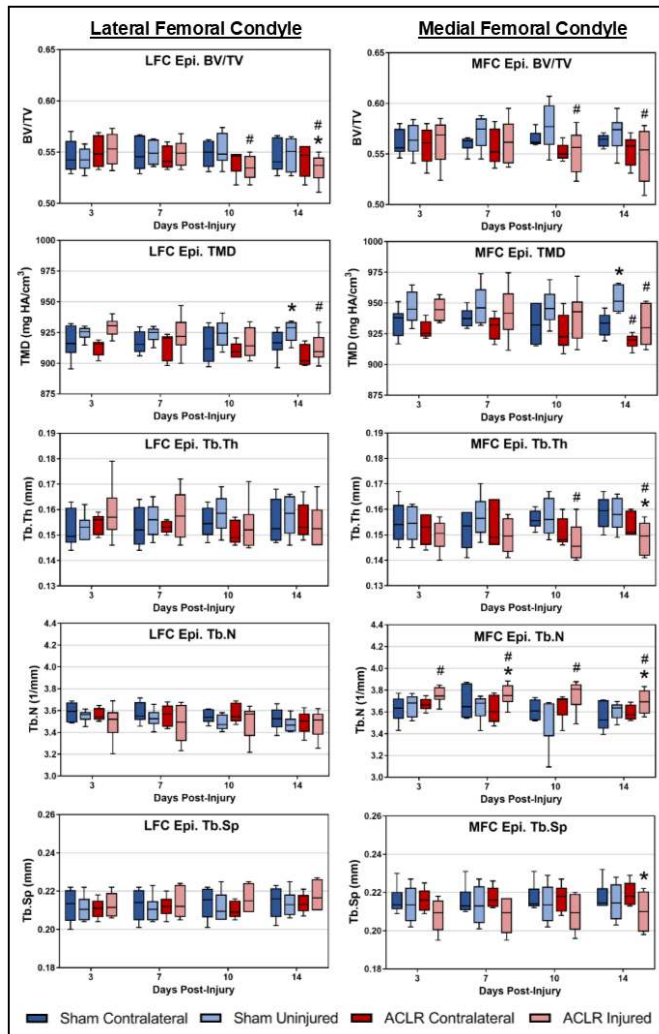
244

Fig 2. Epiphyseal Bone Morphometry of MFC and LFC. Longitudinal, in vivo µCT of
epiphyseal trabecular bone demonstrates that ACLR-induced catabolic remodeling is most
pronounced on the MFC. ACLR induces loss of trabecular BV/TV, compared to Sham femora.
By 14d post-injury, injured ACLR femora exhibit decreased Tb.Th, decreased Tb.Sp, and
increased Tb.N. No changes in Tb.Th, Tb.N, or Tb.Sp were noted in the LFC in either ACLR or
Sham. (n=6 Sham; n=5 ACLR) * indicates significant difference to contralateral limb; #
indicates significant difference to ipsilateral limb in Sham.

252

253   *In vivo NIR molecular imaging reveals reduced bone formation and greater catabolic bone*

254   *turnover following ACLR*

255   To elucidate whether joint injury-induced alterations in bone microstructure are due to

256   dampened anabolic bone formation, due to increased catabolic osteoclast activity, or both, we

257   employed *in vivo* NIR molecular imaging. BoneTag NIR signal – a direct measure of new bone

258   formation – was significantly decreased in ACLR injured limbs at all timepoints compared to

259   contralateral limbs and at 3d, 10d, and 14d compared to Sham uninjured limbs (Fig 3A, B),

260   indicating an immediate and sustained impact of ACLR on bone anabolism. NIR heatmaps

261   demonstrate marked loss of BoneTag signal in ACLR, most notably at the location of the

262   femoral epiphysis, whereas Sham knees exhibit higher, evenly-distributed BoneTag signal

263   throughout the whole joint (Fig 3A). CatK NIR signal – an indirect measure of osteoclast

264   activity[29, 30] – was measured at the final 14d timepoint and found to be significantly increased in

265   ACLR injured limbs compared to both contralateral ACLR limbs and uninjured Sham limbs (Fig

266   3C). CatK heatmaps demonstrate increased signal intensity throughout the entire knee joint in

267   injured ACLR limbs (Fig 3A). To control for compounding BoneTag signal and potential

268   contralateral effects (i.e. reduced activity in ACLR rats), we normalized BoneTag and Cat K

269   signal of the injured/uninjured limbs in ACLR/Sham to their respective contralateral limb.

270   Normalized data indicates a sustained ~15-20% reduction in longitudinal BoneTag signal (Fig

271   3D) and a ~32% increase in CatK signal (Fig 3E) in ACLR, whereas normalized BoneTag and

272   CatK signal in Sham were consistently ~1.

273   To ascertain the relationship between bone anabolism and bone catabolism, we

274   performed bivariate correlations between absolute CatK and BoneTag signal. Analyzing all

275   limbs of both Sham and ACLR yielded a weak, albeit significant inverse correlation (r^2=0.353,

276   *P*=0.002) between CatK and BoneTag signal (Fig 3F). Including only loaded limbs (ACLR

277   injured and Sham uninjured) markedly improved this correlation (r^2=0.610, *P*=0.002) (Fig 3G),

278   indicating an *in vivo* relationship between bone anabolism and catabolism following joint loading

279   in our model. Collectively, this data demonstrates that ACLR is associated with both decreased

280   bone formation (i.e. anabolism) and increased osteoclast activity (i.e. catabolism) and that these

281   processes are inversely correlated *in vivo*.

282
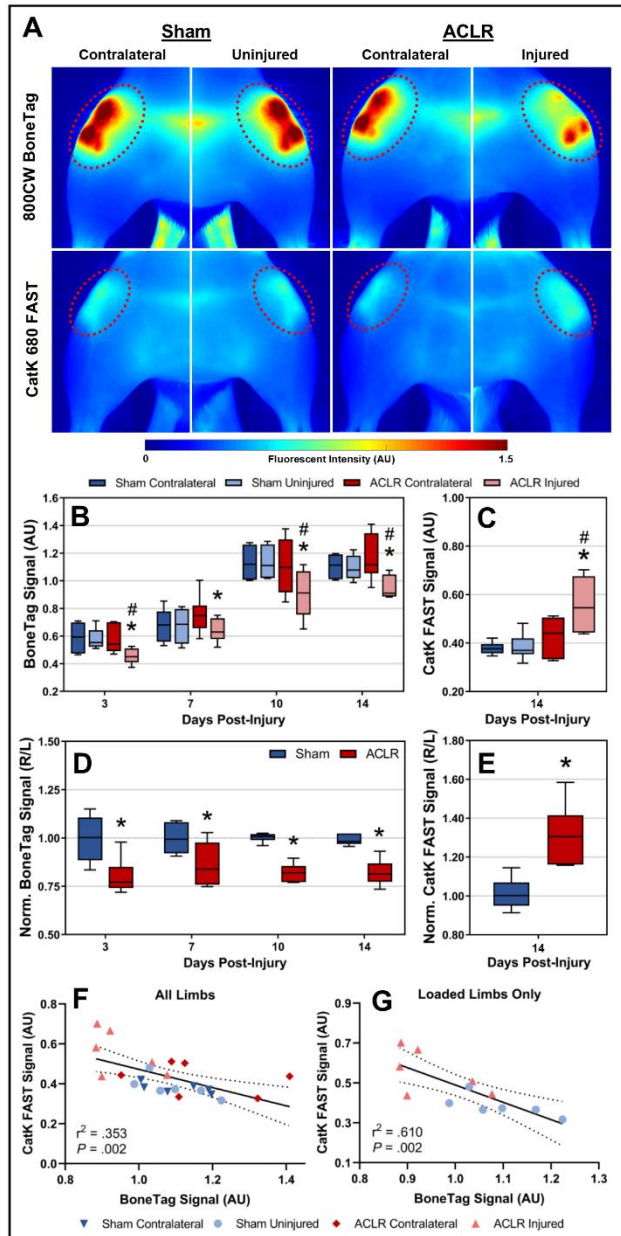
Fig 3. Near-infrared Molecular Imaging of Bone Turnover. NIR heatmaps (A) indicate decreased BoneTag and increased CatK signal in the injured limb of ACLR. Quantitatively, there was a significant reduction in longitudinal BoneTag (B) and significant increase in endpoint CatK (C) signal compared to both Sham ipsilateral and ACLR contralateral limbs (n=6 Sham; n=6 ACLR). Normalized BoneTag (D) and CatK (E) data indicate a ~15-20% reduction and ~32% increase, respectively. A poor correlation between BoneTag and CatK signal was observed when all study limbs were analyzed (F), however including only loaded limbs yielded a

291   moderate inverse correlation, demonstrating the in vivo relationship between bone anabolism and

292   catabolism following ACLR (G). * indicates significant difference to contralateral limb; #

293   indicates significant difference to ipsilateral limb in Sham.

294

295   *Histomorphometry Indicates Thwarted Bone Formation and Increased Osteoclast Number*

296   To label newly-deposited bone and quantitatively assess 14d bone formation, we injected

297   rats with calcein at the beginning and end of the study. Fluorescent microscopy demonstrates

298   reduced overall calcein uptake, a reduced incidence of double calcein labels, and reduced inter-

299   label distance in the epiphyseal trabecular bone of ACLR injured femora (Fig 4A), indicating

300   thwarted bone formation. Uninjured contralateral ACLR femora and both femora of Sham

301   exhibit consistent presence of double labels throughout the epiphysis, indicative of new bone

302   formation. Quantitative measurement of dynamic histomorphometric parameters corroborate the

303   observation of reduced bone formation, and injured ACLR femora had significantly lower

304   epiphyseal MS compared to contralateral limbs and significantly lower BFR/BV compared to

305   uninjured, Sham limbs (Fig 4B). There were no significant differences in epiphyseal MS/BS and

306   MAR (Fig 4B).

307   TRAP-stained slides were analyzed to quantify osteoclast density within the distal

308   femoral epiphysis. Qualitatively, all groups exhibited greater osteoclast numbers in SCB (Fig 4C,

309   left column) compared to trabecular bone (Fig 4C, right column). Injured ACLR femora had

310   more abundant osteoclasts, most notably in or near SCB (Fig 4C, left column) – osteoclasts were

311   commonly observed penetrating calcified cartilage and, in some instances, spanning the tidemark

312   (Fig 4C). Quantitatively, ACLR injured femora had significantly higher N.Oc/T.Ar compared to

313   both ACLR Contralateral and Sham Uninjured and significantly higher N.Oc/BS compared to

314   ACLR Contralateral (Fig 4D). Taken together, histomorphometric assessments demonstrate that

315   ACLR thwarts new bone formation and induces osteoclast infiltration in epiphyseal bone, most

316   notably in the subchondral compartment.
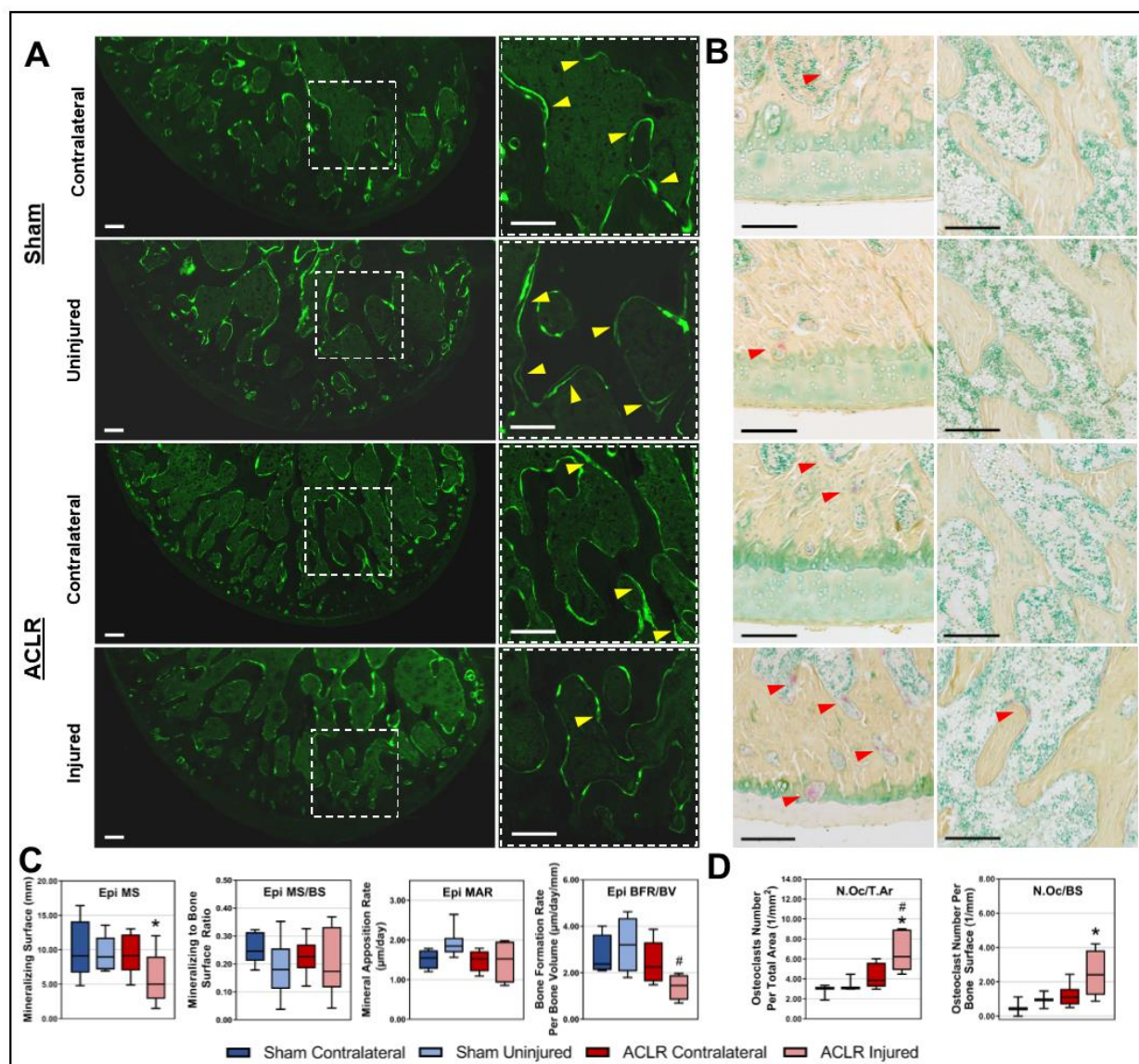
317

318   **Fig 4. Histomorphometry of Bone Formation and Osteoclast Density.** Fluorescent sections

319   (A) demonstrate consistent presence of double calcein labels (yellow arrowheads) in both Sham

320   limbs and in the ACLR contralateral limb. The ACLR injured limb exhibits an overall reduced

321   calcein uptake and a lower incidence of double labels, indicating thwarted bone formation.

322   Quantitatively, ACLR Injured limbs exhibit reductions in epiphyseal MS and BFR/BV (n=5

323   Sham; n=6 ACLR) (C). Brightfield imaging of TRAP-stained sections indicate increased

324   osteoclast numbers in ACLR Injured femora (B). Osteoclasts (red arrowheads) were most

325   numerous in subchondral bone (B, left column) compared to epiphyseal trabecular bone (B, right

326   column). Quantitatively, ACLR Injured femora had significantly elevated N.Oc/T.Ar and

327   N.Oc/BS (n=3 Sham; n=6 ACLR) (D). * indicates significant difference to contralateral limb; #

328   indicates significant difference to ipsilateral limb in Sham. Calcein images scalebar is 250 μm.

329   TRAP images scalebar is 150 μm.

330

331   *Early Articular Cartilage Damage is Primarily Confined to the MFC following ACLR*

332   To contextualize bone-related findings with the degree/severity of cartilage degeneration

333   at the acute 14d timepoint after ACL injury, we analyzed femoral AC using contrast-enhanced

334   μCT and sagittal Saf-O-stained histology. Histologically, femoral cartilage of both Sham limbs

335   appeared normal with no alterations in structure, cellular phenotype, or staining intensity (Fig

336   5A). Minor cartilage damage, most commonly superficial fibrillation, was observed on the MFC

337   of ACLR contralateral femora (Fig 5A). The MFC of ACLR injured femora exhibited marked

338   cartilage damage and degeneration, with the anterior condyle exhibiting structure damage,

339   cartilage erosion, hypocellularity, and loss of Saf-O staining. The posterior condyle exhibited

340   notable swelling, increased chondrocyte cloning and clustering, and damage to the superficial

341   zone (Fig 5A). Compared to both ACLR contralateral and Sham ipsilateral, ACLR injured

342   femora had significantly greater MFC and whole-femur OARSI score, with marginal but non-

343   significant increases in OARSI score on the LFC (Fig 5C). Contrast-enhanced μCT thickness

344   maps corroborate histological findings: Sham femora exhibit a generally congruent articular

345   surface with normal zones of increased cartilage thickness at the weight-bearing regions of the

346   condyles (Fig 5B). Injured ACLR femora exhibit abnormal cartilage thickness distributions,

347   most notably on the MFC, where zones of markedly-increased cartilage thickness were observed

348   at the central weight-bearing region and zones of markedly-decreased cartilage thickness were

349   observed at the anterior aspect (Fig 5B). Quantitatively, both condyles of injured ACLR limbs

350   exhibited significant increases in mean cartilage thickness of ~20-30% compared to uninjured

351   contralateral and Sham limbs (Fig 5D). Lastly, injured ACLR femora exhibited a significant

352   ~75-95% increase in MFC S_a and a significant ~50-60% increase in whole-femur S_a (Fig 5E).

353   Due to only cartilage thickening and no observed cartilage loss on the LFC of ACLR injured

354   femora, there was no significant increase in LFC S_a (Fig 5E). Both Sham femora and the ACLR

355   contralateral femora exhibited similar cartilage thickness and S_a (Fig 5D,E).

356
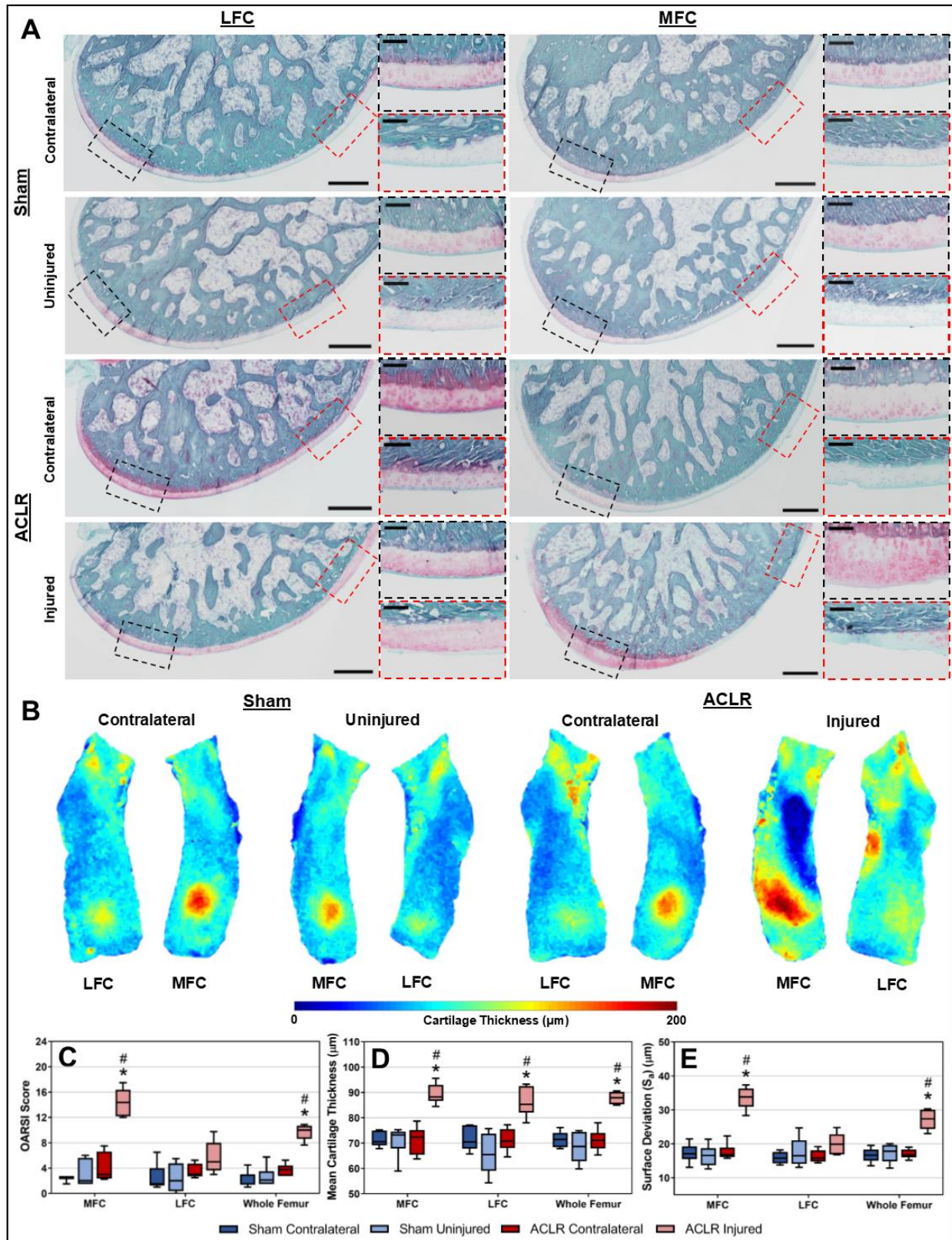
358 **Fig 5. Articular Cartilage Damage and Degeneration.** Histologically, the MFC and LFC of

359 both limbs in Sham exhibit congruent articular cartilage with normal cellular morphology and

360 staining intensity (A). Minor superficial cartilage damage was observed on the MFC of ACLR

361 contralateral limbs. ACLR injured femora exhibited marked structural damage and

362 hypocellularity on the anterior MFC, with swelling and abnormal chondrocyte clustering on the

363 posterior MFC. The LFC of ACLR injured femora exhibited swelling and superficial damage.

364 CE-μCT confirms histological observations by demonstrating drastic alterations in cartilage

365 thickness distributions on the MFC of ACLR injured (B). ACLR injured femora had significantly

366 increased OARSI score (n=6 Sham; n=6 ACLR) (C), increased femoral cartilage thickness (D),

367 and increased femoral cartilage surface deviation (E). * indicates significant difference to

368 contralateral limb; # indicates significant difference to ipsilateral limb in Sham. Scalebar of

369 whole-condyle images is 500 μm. Scalebar of high-magnification images is 200 μm.

370

371

372 **DISCUSSION:**

373   This study sought to characterize acute alterations to trabecular and SCB in a rat model of

374 noninvasive ACL rupture, and assess whether alterations in bone precede measurable cartilage

375 changes. Our results demonstrate that in this model, rapid alterations to SCB and trabecular bone

376 turnover and microstructure are observed immediately after injury. Despite evidence of catabolic

377 bone remodeling as early as 3-7 days post-injury, our findings also indicate notable damage to

378 cartilage of the MFC in ACL-injured femora by 14 days post-injury. Thus, given the magnitude

379 of cartilage damage, we do not conclude that bony changes markedly precede AC degeneration

380 in this model. Collectively, our results demonstrate that the acute bone loss observed after

381 traumatic joint injury is driven by both thwarted anabolism (based on NIR BoneTag and dynamic

382   histomorphometry results) and increased catabolism (based on NIR CatK and TRAP histology

383   results).

384   　　　Prior clinical studies have demonstrated a compartment/region-dependent loss of

385   periarticular bone mass and/or bone mineral density following traumatic joint injury[37-42]. Several

386   of these studies indicate incomplete recovery of bony deficits in the long-term, with some

387   evidence even indicating lower BMD in the injured limb 10+ years after knee injury.[40] A recent

388   study which first employed high-resolution CT in humans with ACL injury demonstrated the

389   microstructural nature of injury-induced bone loss[42], largely corroborating our observations in

390   rats. Collectively, these data point towards a phenotypic shift in periarticular bone and long-term

391   imbalance between tissue anabolism and catabolism. The present study supports this premise, as

392   our data demonstrate that ACLR markedly thwarts bone formation/anabolism and activates bone

393   resorption/catabolism, leading to complex, region-dependent remodeling. Histologically, this

394   response was characterized by decreased bone deposition and increased osteoclast numbers.

395   While this remodeling is largely characterized by bone loss, our analysis of LFC SCB indicates a

396   small but significant increase in SCB BV/TV and TMD. This evidence of a compartment/region-

397   dependent bone remodeling response to injury points towards the complexity of PTOA

398   pathogenesis and the importance of evaluating the entire joint in its individual regions when

399   characterizing pathophysiology and evaluating therapeutic strategies.

400   　　　While chronic joint destabilization is known to induce progressive cartilage degeneration,

401   it remains unclear whether the damage observed on the MFC in this ACLR model (and similar

402   models in mice[22]) is primarily due to chronic instability or due to acute structural damage from

403   injury loading. Our present findings indicate a similar, albeit less severe cartilage phenotype on

404   the MFC at this early 14-day timepoint as previously observed at both 4 and 10 weeks post-

405   ACLR in our prior studies[26]. Interestingly, the same overall phenotype was also observed in a rat

406   surgical ACL transection model, employed as a comparison in the same prior study[26], which

407   lacks injurious mechanical loading. Thus, we conclude that ACL deficiency-induced joint

408   destabilization has an immediate impact on the onset of cartilage degeneration in this model, that

409   this degeneration is concurrent with bony remodeling, and that it is not just the acute trauma to

410   cartilage during the injurious subluxation and overloading event that induces the observed

411   phenotype on the MFC. While synovitis – a non-mechanical contributor to PTOA pathogenesis –

412   is known to also initiate cartilage degeneration via cytokines, chemokines, and tissue proteases,

413   these effects would not be expected to be region-dependent. Thus, the drastic differences in

414   cartilage phenotype on the anterior vs posterior MFC may be attributable to primarily

415   mechanical factors. It is also possible that proinflammatory cytokines and proteases expressed by

416   synovium differentially accelerate extracellular matrix damage in chondrocytes that undergo

417   pathological loading conditions.

418   Our findings stress the importance of evaluating both the contralateral limb of the injured

419   rat and a limb from a sham-loaded rat in this PTOA model. While contralateral bone and

420   cartilage changes were subtle, they nonetheless were observable. Reduced activity leading to

421   offloading of both limbs following joint injury, in addition to contralateral compensation and gait

422   changes may confound interpretation of tissue changes in the injured limb if only compared to

423   the contralateral limb. Future studies should avoid bilateral ACLR and employ appropriate

424   controls.

425   This study is not without limitations. Our conclusion regarding the temporal relationship

426   between AC degeneration and bone remodeling are based on a single endpoint assessment of

427   AC, given the technical limitations of contrast-enhanced imaging and the destructive nature of

428 histology. Future studies may develop *in vivo* contrast-enhanced imaging approaches to

429 longitudinally assess AC morphology. Although our rigorous image analysis methodology

430 sought to eliminate subjective user input via registration-based algorithms, our workflow

431 nonetheless relied on some manual tissue contouring. Our histomorphometry and NIR data

432 demonstrates thwarted bone formation, however we did not perform histologic osteoblast counts

433 to determine whether this effect is driven by a reduction in osteoblast activity or overall

434 osteoblast numbers.

435   In a study combining multi-disciplinary imaging, histological and histomorphometric

436 measures to characterize acute joint injury-induced bone and cartilage remodeling, we found that

437 noninvasive ACLR in the rat induces immediate and sustained reduction of bone anabolism and

438 an overactivation of bone catabolism. Future studies in our group aim to elucidate how intra-

439 articular inflammation promotes this phenotype in order to uncover the molecular mechanisms of

440 degenerative tissue changes, facilitating the development of novel PTOA treatments.

REFERENCES:

1. L. Lohmander, A. Östenberg, M. Englund, and H. Roos, High prevalence of knee osteoarthritis, pain, and functional limitations in female soccer players twelve years after anterior cruciate ligament injury. *Arthritis & Rheumatism* **50** (10), 2004, 3145-3152.

2. L.S. Lohmander, P.M. Englund, L.L. Dahl, and E.M. Roos, The long-term consequence of anterior cruciate ligament and meniscus injuries: osteoarthritis. *Am J Sports Med* **35** (10), 2007, 1756-1769.

3. A. Carbone, and S. Rodeo, Review of current understanding of post-traumatic osteoarthritis resulting from sports injuries. *Journal of orthopaedic research* **35** (3), 2017, 397-405.

4. M. Kessler, H. Behrend, S. Henz, G. Stutz, A. Rukavina, and M. Kuster, Function, osteoarthritis and activity after ACL-rupture: 11 years follow-up results of conservative versus reconstructive treatment. *Knee Surgery, Sports Traumatology, Arthroscopy* **16** (5), 2008, 442-448.

5. B. Luc, P.A. Gribble, and B.G. Pietrosimone, Osteoarthritis prevalence following anterior cruciate ligament reconstruction: a systematic review and numbers-needed-to-treat analysis. *Journal of athletic training* **49** (6), 2014, 806-819.

6. R.J. Lories, and F.P. Luyten, The bone–cartilage unit in osteoarthritis. *Nature Reviews Rheumatology* **7** (1), 2011, 43.

7. S.R. Goldring, and M.B. Goldring, Changes in the osteochondral unit during osteoarthritis: structure, function and cartilage–bone crosstalk. *Nature Reviews Rheumatology* **12** (11), 2016, 632.

8. D.B. Burr, and M.A. Gallant, Bone remodelling in osteoarthritis. *Nature Reviews Rheumatology* **8** (11), 2012, 665.

9. J. Pan, B. Wang, W. Li, X. Zhou, T. Scherr, Y. Yang, et al., Elevated cross-talk between subchondral bone and cartilage in osteoarthritic joints. *Bone* **51** (2), 2012, 212-217.

10. S.R. Goldring, Alterations in periarticular bone and cross talk between subchondral bone and articular cartilage in osteoarthritis. *Therapeutic advances in musculoskeletal disease* **4** (4), 2012, 249-258.

11. J. Lu, H. Zhang, D. Cai, C. Zeng, P. Lai, Y. Shao, et al., Positive-Feedback Regulation of Subchondral H-Type Vessel Formation by Chondrocyte Promotes Osteoarthritis Development in Mice. *Journal of Bone and Mineral Research* **33** (5), 2018, 909-920.

12. P. Van der Kraan, and W. Van den Berg, Chondrocyte hypertrophy and osteoarthritis: role in initiation and progression of cartilage degeneration? *Osteoarthritis and cartilage* **20** (3), 2012, 223-232.

13. J. Huebner, M. Hanes, B. Beekman, J. TeKoppele, and V. Kraus, A comparative analysis of bone and cartilage metabolism in two strains of guinea-pig with varying degrees of naturally occurring osteoarthritis. *Osteoarthritis and cartilage* **10** (10), 2002, 758-767.

14. T. Wang, C.-Y. Wen, C.-H. Yan, W.-W. Lu, and K.-Y. Chiu, Spatial and temporal changes of subchondral bone proceed to microscopic articular cartilage degeneration in guinea pigs with spontaneous osteoarthritis. *Osteoarthritis and cartilage* **21** (4), 2013, 574-581.

15. T. Hügle, and J. Geurts, What drives osteoarthritis?—Synovial versus subchondral bone pathology. *Rheumatology* **56** (9), 2016, 1461-1471.

16. J.B. Driban, R.J. Ward, C.B. Eaton, G.H. Lo, L.L. Price, B. Lu, et al., Meniscal extrusion or subchondral damage characterize incident accelerated osteoarthritis: data from the Osteoarthritis Initiative. *Clinical Anatomy* **28** (6), 2015, 792-799.

17. G. Schett, Effects of inflammatory and anti-inflammatory cytokines on the bone. *European journal of clinical investigation* **41** (12), 2011, 1361-1366.

| 495 | 18. | M.J. Anderson, S. Diko, L.M. Baehr, K. Baar, S.C. Bodine, and B.A. Christiansen, Contribution of mechanical unloading to trabecular bone loss following non-invasive knee injury in mice. *Journal of Orthopaedic Research* **34** (10), 2016, 1680-1687. |

495 18. M.J. Anderson, S. Diko, L.M. Baehr, K. Baar, S.C. Bodine, and B.A. Christiansen, Contribution of
496 mechanical unloading to trabecular bone loss following non-invasive knee injury in mice. *Journal*
497 *of Orthopaedic Research* **34** (10), 2016, 1680-1687.
498 19. T. Funck-Brentano, W. Bouaziz, C. Marty, V. Geoffroy, E. Hay, and M. Cohen-Solal, Dkk-1–
499 Mediated Inhibition of Wnt Signaling in Bone Ameliorates Osteoarthritis in Mice. *Arthritis &*
500 *rheumatology* **66** (11), 2014, 3028-3039.
501 20. W. Bouaziz, T. Funck-Brentano, H. Lin, C. Marty, H.-K. Ea, E. Hay, et al., Loss of sclerostin
502 promotes osteoarthritis in mice via β-catenin-dependent and-independent Wnt pathways.
503 *Arthritis research & therapy* **17** (1), 2015, 24.
504 21. F.P. Luyten, P. Tylzanowski, and R.J. Lories, Wnt signaling and osteoarthritis. *Bone* **44** (4), 2009,
505 522-527.
506 22. B.A. Christiansen, M. Anderson, C.A. Lee, J. Williams, J. Yik, and D.R. Haudenschild,
507 Musculoskeletal changes following non-invasive knee injury using a novel mouse model of post-
508 traumatic osteoarthritis. *Osteoarthritis and cartilage* **20** (7), 2012, 773-782.
509 23. A. Ramme, M. Lendhey, J. Raya, T. Kirsch, and O. Kennedy, A novel rat model for subchondral
510 microdamage in acute knee injury: a potential mechanism in post-traumatic osteoarthritis.
511 *Osteoarthritis and cartilage* **24** (10), 2016, 1776-1785.
512 24. C.T.G. Appleton, D.D. McErlain, V. Pitelka, N. Schwartz, S.M. Bernier, J.L. Henry, et al., Forced
513 mobilization accelerates pathogenesis: characterization of a preclinical surgical model of
514 osteoarthritis. *Arthritis research & therapy* **9** (1), 2007, R13.
515 25. T. Maerz, M. Kurdziel, M. Newton, P. Altman, K. Anderson, H. Matthew, et al., Subchondral and
516 epiphyseal bone remodeling following surgical transection and noninvasive rupture of the
517 anterior cruciate ligament as models of post-traumatic osteoarthritis. *Osteoarthritis and*
518 *cartilage* **24** (4), 2016, 698-708.
519 26. T. Maerz, M. Newton, M. Kurdziel, P. Altman, K. Anderson, H. Matthew, et al., Articular cartilage
520 degeneration following anterior cruciate ligament injury: a comparison of surgical transection
521 and noninvasive rupture as preclinical models of post-traumatic osteoarthritis. *Osteoarthritis*
522 *and cartilage* **24** (11), 2016, 1918-1927.
523 27. T. Maerz, M.D. Kurdziel, A.A. Davidson, K.C. Baker, K. Anderson, and H.W. Matthew,
524 Biomechanical characterization of a model of noninvasive, traumatic anterior cruciate ligament
525 injury in the rat. *Annals of biomedical engineering* **43** (10), 2015, 2467-2476.
526 28. J.L. Kovar, X. Xu, D. Draney, A. Cupp, M.A. Simpson, and D.M. Olive, Near-infrared-labeled
527 tetracycline derivative is an effective marker of bone deposition in mice. *Analytical biochemistry*
528 **416** (2), 2011, 167-173.
529 29. K.M. Kozloff, L. Quinti, S. Patntirapong, P.V. Hauschka, C.-H. Tung, R. Weissleder, et al., Non-
530 invasive optical detection of cathepsin K-mediated fluorescence reveals osteoclast activity in
531 vitro and in vivo. *Bone* **44** (2), 2009, 190-198.
532 30. P.B. Satkunananthan, M.J. Anderson, N.M. De Jesus, D.R. Haudenschild, C.M. Ripplinger, and
533 B.A. Christiansen, In vivo fluorescence reflectance imaging of protease activity in a mouse model
534 of post-traumatic osteoarthritis. *Osteoarthritis and cartilage* **22** (10), 2014, 1461-1469.
535 31. D. Sage, D. Prodanov, J.-Y. Tinevez, and J. Schindelin. MIJ: making interoperability between
536 ImageJ and Matlab possible. ImageJ User & Developer Conference 2012. doi:
537 32. M. Doube, M.M. Kłosowski, I. Arganda-Carreras, F.P. Cordelières, R.P. Dougherty, J.S. Jackson, et
538 al., BoneJ: free and extensible bone image analysis in ImageJ. *Bone* **47** (6), 2010, 1076-1079.
539 33. T. Maerz, M. Newton, H. Matthew, and K. Baker, Surface roughness and thickness analysis of
540 contrast-enhanced articular cartilage using mesh parameterization. *Osteoarthritis and cartilage*
541 **24** (2), 2016, 290-298.

542 34.   P. Mullen, Y. Tong, P. Alliez, and M. Desbrun. Spectral conformal parameterization. Computer
543   Graphics Forum 2008; 1487-1494. doi:
544 35.   N. Gerwin, A. Bendele, S. Glasson, and C.S. Carlson, The OARSI histopathology initiative–
545   recommendations for histological assessments of osteoarthritis in the rat. *Osteoarthritis and*
546   *Cartilage* **18**, 2010, S24-S34.
547 36.   D.W. Dempster, J.E. Compston, M.K. Drezner, F.H. Glorieux, J.A. Kanis, H. Malluche, et al.,
548   Standardized nomenclature, symbols, and units for bone histomorphometry: a 2012 update of
549   the report of the ASBMR Histomorphometry Nomenclature Committee. *Journal of bone and*
550   *mineral research* **28** (1), 2013, 2-17.
551 37.   J. Leppälä, P. Kannus, A. Natri, M. Pasanen, H. Sievänen, I. Vuori, et al., Effect of anterior cruciate
552   ligament injury of the knee on bone mineral density of the spine and affected lower extremity: a
553   prospective one-year follow-up study. *Calcified tissue international* **64** (4), 1999, 357-363.
554 38.   B. Zerahn, A.O. Munk, J. Helweg, and C. Hovgaard, Bone mineral density in the proximal tibia
555   and calcaneus before and after arthroscopic reconstruction of the anterior cruciate ligament.
556   *Arthroscopy: The Journal of Arthroscopic & Related Surgery* **22** (3), 2006, 265-269.
557 39.   A. Bayar, S. Sarıkaya, S. Keser, Ş. Özdolap, İ. Tuncay, and A. Ege, Regional bone density changes
558   in anterior cruciate ligament deficient knees: a DEXA study. *The Knee* **15** (5), 2008, 373-377.
559 40.   P. Kannus, H. Sievänen, M. Järvinen, A. Heinonen, P. Oja, and I. Vuori, A cruciate ligament injury
560   produces considerable, permanent osteoporosis in the affected knee. *Journal of bone and*
561   *mineral research* **7** (12), 1992, 1429-1434.
562 41.   B. van Meer, J. Waarsing, W. van Eijsden, D. Meuffels, E. van Arkel, J. Verhaar, et al., Bone
563   mineral density changes in the knee following anterior cruciate ligament rupture. *Osteoarthritis*
564   *and cartilage* **22** (1), 2014, 154-161.
565 42.   A. Kroker, B.A. Besler, J.L. Bhatla, M. Shtil, P. Salat, N. Mohtadi, et al., Longitudinal Effects of
566   Acute Anterior Cruciate Ligament Tears on Peri-Articular Bone in Human Knees Within the First
567   Year of Injury. *Journal of Orthopaedic Research®* **37** (11), 2019, 2325-2336.

568

569 **FIGURE LEGENDS:**

570 **Fig 1. Subchondral and Metaphyseal Bone Morphometry**. Three-dimensional thickness maps
571 demonstrate compartment-dependent alterations in SCB morphometry and catabolic remodeling
572 of metaphyseal trabecular bone following ACLR (A). Compared to Sham, ACLR had lower SCB
573 BV/TV and TMD on the MFC in both limbs, whereas the LFC of injured ACLR knees exhibited
574 BV/TV and TMD gains (n=6 Sham; n=5 ACLR) (B). Both ACLR and Sham induced SCB
575 thinning on the MFC, compared to contralateral knees (B). MFC thinning in Sham was confined
576 to the anterior condyle, whereas the ACLR MFC exhibits thinning throughout the entire condyle
577 (B). ACLR also induced catabolic remodeling of metaphyseal trabecular bone (n=6 Sham; n=6
578 ACLR) (A,C). * indicates significant difference to contralateral limb; # indicates significant
579 difference to ipsilateral limb in Sham.

580

581 **Fig 2. Epiphyseal Bone Morphometry of MFC and LFC**. Longitudinal, in vivo μCT of

582 epiphyseal trabecular bone demonstrates that ACLR-induced catabolic remodeling is most

583 pronounced on the MFC. ACLR induces loss of trabecular BV/TV, compared to Sham femora.

584 By 14d post-injury, injured ACLR femora exhibit decreased Tb.Th, decreased Tb.Sp, and

585 increased Tb.N. No changes in Tb.Th, Tb.N, or Tb.Sp were noted in the LFC in either ACLR or

586 Sham. (n=6 Sham; n=5 ACLR) * indicates significant difference to contralateral limb; #

587 indicates significant difference to ipsilateral limb in Sham.

588

589 **Fig 3. Near-infrared Molecular Imaging of Bone Turnover.** NIR heatmaps (A) indicate

590 decreased BoneTag and increased CatK signal in the injured limb of ACLR. Quantitatively, there

591 was a significant reduction in longitudinal BoneTag (B) and significant increase in endpoint

592 CatK (C) signal compared to both Sham ipsilateral and ACLR contralateral limbs (n=6 Sham;

593 n=6 ACLR). Normalized BoneTag (D) and CatK (E) data indicate a ~15-20% reduction and

594 ~32% increase, respectively. A poor correlation between BoneTag and CatK signal was observed

595 when all study limbs were analyzed (F), however including only loaded limbs yielded a

596 moderate inverse correlation, demonstrating the in vivo relationship between bone anabolism and

597 catabolism following ACLR (G). * indicates significant difference to contralateral limb; #

598 indicates significant difference to ipsilateral limb in Sham.

599 **Fig 4. Histomorphometry of Bone Formation and Osteoclast Density.** Fluorescent sections

600 (A) demonstrate consistent presence of double calcein labels (yellow arrowheads) in both Sham

601 limbs and in the ACLR contralateral limb. The ACLR injured limb exhibits an overall reduced

602 calcein uptake and a lower incidence of double labels, indicating thwarted bone formation.

603 Quantitatively, ACLR Injured limbs exhibit reductions in epiphyseal MS and BFR/BV (n=5

604 Sham; n=6 ACLR) (C). Brightfield imaging of TRAP-stained sections indicate increased

605 osteoclast numbers in ACLR Injured femora (B). Osteoclasts (red arrowheads) were most

606 numerous in subchondral bone (B, left column) compared to epiphyseal trabecular bone (B, right

607 column). Quantitatively, ACLR Injured femora had significantly elevated N.Oc/T.Ar and

608 N.Oc/BS (n=3 Sham; n=6 ACLR) (D). * indicates significant difference to contralateral limb; #

609   indicates significant difference to ipsilateral limb in Sham. Calcein images scalebar is 250 μm.

610   TRAP images scalebar is 150 μm.

611

612   **Fig 5. Articular Cartilage Damage and Degeneration.** Histologically, the MFC and LFC of

613   both limbs in Sham exhibit congruent articular cartilage with normal cellular morphology and

614   staining intensity (A). Minor superficial cartilage damage was observed on the MFC of ACLR

615   contralateral limbs. ACLR injured femora exhibited marked structural damage and

616   hypocellularity on the anterior MFC, with swelling and abnormal chondrocyte clustering on the

617   posterior MFC. The LFC of ACLR injured femora exhibited swelling and superficial damage.

618   CE-μCT confirms histological observations by demonstrating drastic alterations in cartilage

619   thickness distributions on the MFC of ACLR injured (B). ACLR injured femora had significantly

620   increased OARSI score (n=6 Sham; n=6 ACLR) (C), increased femoral cartilage thickness (D),

621   and increased femoral cartilage surface deviation (E). * indicates significant difference to

622   contralateral limb; # indicates significant difference to ipsilateral limb in Sham. Scalebar of

623   whole-condyle images is 500 μm. Scalebar of high-magnification images is 200 μm.

624